HHS Public Access

Author manuscript

Nat Med. Author manuscript; available in PMC 2016 March 01.

Published in final edited form as:

Nat Med. 2015 September ; 21(9): 1091–1100. doi:10.1038/nm.3929.

In vivo imaging and tracking of host-microbiota interactions via metabolic labeling of gut anaerobic bacteria

Naama Geva-Zatorsky[1,*], **David Alvarez**[1,*], **Jason E. Hudak**[1], **Nicola C. Reading**[1,†], **Deniz Erturk-Hasdemir**[1], **Suryasarathi Dasgupta**[1], **Ulrich H. von Andrian**[1,2], and **Dennis L. Kasper**[1,§]

[1]Department of Microbiology and Immunobiology, Harvard Medical School, Boston, Massachusetts USA

[2]The Ragon Institute of Massachusetts General Hospital, Massachusetts Institute of Technology, and Harvard

Abstract

The intestine is densely populated by anaerobic commensal bacteria. These microorganisms shape immune system development, but our understanding of host–commensal interactions is hampered by a lack of tools for studying the anaerobic intestinal environment. We applied metabolic oligosaccharide engineering and bioorthogonal click-chemistry to label various commensal anaerobes, including *Bacteroides fragilis*, a common and immunologically important commensal. We studied the dissemination of *B. fragilis* following acute peritonitis, and characterized the interactions of the intact microbe and its polysaccharide components in myeloid and B cell lineages. The distribution and colonization of labeled *B. fragilis* along the intestine can be assessed, as well as niche competition following coadministration of multiple species of the microbiota. Nine additional anaerobic commensals (both gram-negative and gram-positive) from three phyla common in the gut—Bacteroidetes, Firmicutes, and Proteobacteria—and five families and one aerobic pathogen (*Staphylococcus aureus*) were also fluorescently labeled. This strategy permits visualization of the anaerobic microbial niche by various methods, including intravital two-photon microscopy and non-invasive whole-body imaging, and an approach to study microbial colonization and host–microbe interactions in real-time.

Introduction

The human gastrointestinal tract is densely populated by >10^{13} bacteria, which have coevolved to play important roles in human health and disease[1–6]. Despite many benefits of

[§]Corresponding author: dennis_kasper@hms.harvard.edu.
[*]These authors contributed equally to this work.
[†]Current affiliation: Envision Communications, Fort Worth, Texas, USA

Author Contributions

N.G-Z. and D.A. designed the experiments, analyzed the data, and wrote the manuscript with help from J.E.H. and N.C.R. D.E-H. and S.D. provided experimental help and expertise. D.L.K. supervised the study, edited the manuscript, and provided helpful comments, with assistance from U.H.vA.

Competing financial interests

The authors declare no competing financial interests.

the microbiota[6–9], its dysregulation can cause diseases such as inflammatory bowel disease[10] and autoimmunity[11]. Although research in germ-free[12] (GF) mice established critical roles for the microbiota as a whole, the contribution of single bacterial species and their molecular components has been more difficult to dissect. Although certainly worthwhile, the development of tools that permit a selected species to be labeled, followed, and studied in the context of a diverse microbiota is challenging.

Bacterium-derived polysaccharides and glycoproteins provide modes of communication that are pivotal in bacterial-host cross-talk[13]. To study these components, we chose *Bacteroides fragilis*, a gram-negative obligate anaerobe and common gut commensal, which affects the host immune system via glycans[14]. *B. fragilis* produces eight capsular polysaccharides (A–H) and many glycoproteins[15], and its colonization depends on the presence of at least one polysaccharide[16]. Polysaccharide A (PSA) exerts immunomodulation such as correcting T helper type 1 and 2 imbalances, inducing regulatory T cells, and inducing protective interleukin (IL)-10 responses in models of colitis and experimental autoimmune encephalomyelitis[14,17,18]. The mechanisms underlying immunoprotection remain uncharacterized, including which immune cells interact with live organisms, how bacterial polysaccharides are shed, and where in the intestine they are presented to the immune system. Although fluorescent PSA has been used previously[14], it has not provided a physiological view of a live symbiont's interaction with the host. Addressing these questions in a temporal-spatial manner requires labeling and tracking of *B. fragilis* and, if possible, its glycan components. Conventional fluorescent labeling is useful, though challenging because fluorescent proteins require aerobic conditions[19,20] but most gut commensals are anaerobes, and many labeling methods are based on genetic techniques that target proteins, not polysaccharides.

To overcome these limitations, we utilized metabolic oligosaccharide engineering (MOE) and bioorthogonal click-chemistry (BCC)[21] to label and track live *B. fragilis* and its polysaccharides. A small functional group is incorporated into biomolecules via the cell's endogenous biosynthetic machinery, which rapidly reacts with a second chemical group by BCC, forming a stable covalent bond[22]. This technique has been successful in studies of glycoconjugates and polysaccharides in living systems[23], including prokaryotic organisms[24,25]. We aimed to extend its application to *in vivo* studies of host–commensal interactions in the anaerobic intestine

We report that *B. fragilis* readily incorporates azide-containing non-natural sugars into its natural carbohydrate structures—specifically, PSA. We labeled and tracked *B. fragilis* and its capsular polysaccharides in mice *in vitro* and *in vivo* after acute peritonitis and in its natural intestinal niche. We showed that this method is compatible with advanced imaging technologies, and applied it to nine additional gut anaerobic commensals from five genera, as well as a common aerobic pathogen, *Staphylococcus aureus*. Finally, we used this technique to differentiate and track three anaerobic gut commensal species administered simultaneously, showing its applicability to studies of niche preferences and competition.

Results

Generation of fluorescently labeled B. fragilis by MOE

We incorporated azide functional groups into newly synthesized polysaccharides by supplementing bacterial growth medium with azide-modified sugars. (Fig. 1a). We predicted *B. fragilis* would uptake azide-modified tetraacetylated-N-azidoacetylgalactosamine (GalNAz), since. PSA—the most abundant polysaccharide of *B. fragilis*—comprises repeating units of N-acetyl-galactosamine (GalNAc)[26]. We grew *B. fragilis* in D-GalNAz-supplemented media, then incubated bacteria with fluorescent alkyne or dibenzocyclooctyne (DIBO) derivatives via copper-dependent or copper-independent reactions, respectively. By flow cytometry, we measured higher fluorescence in the copper-dependent labeling reaction (Fig. 1b). Copper catalysis can be toxic to cells; we found a decrease in viability after copper-dependent labeling (Fig. 1c). Since our goal was to track live organisms, we incorporated labeling techniques using copper-independent DIBO derivatives. The use of DIBO derivatives resulted in higher mean fluorescence intensity (MFI) after longer incubation (Fig. 1b) and no toxicity (Fig. 1c). Labeling was specific for GalNAz incorporation, as D-galactose supplementation did not induce fluorescence (Fig. 1d). Moreover, GalNaz supplementation in regular glucose-rich media remained amenable to labeling, suggesting bacteria can be grown under “optimal” conditions without measurable impact from azido-sugar supplementation.

We determined whether other azide-modified glucosamine, mannosamine, and fucose analogs allowed for labeling of *B. fragilis*. Organisms grown with GlcNAz, ManNAz, or FucNAz, had lower MFI than those grown with GalNAz (Fig. 1e), suggesting GalNAz as the most efficient azido-sugar for MOE-BCC labeling of *B. fragilis*, and implying preferential—not universal—labeling of a unique carbohydrate.

We studied fluorescence dilution during bacterial growth, analogous to use of carboxyfluorescein succinimidyl ester in proliferating eukaryotic cells[27]. Under optimal growth conditions, fluorescently labeled bacteria gradually lost fluorescence over the first 8 h reaching a plateau at 8–24 h (Fig. 1f), with a calculated fluorescence half-life during log phase of approximately 1.6 h. Fluorescence loss coincided with increased bacterial counts during log phase with no measurable growth defects associated with fluorescent labeling (Fig. 1g).

Surface polysaccharide expression and phase variation is important for *B. fragilis* colonization [28]. However, the kinetics of carbohydrate shedding, turnover, and production are unknown. We performed sequential labeling, whereby *B. fragilis* was initially labeled with AF488-DIBO, grown overnight in regular conditions supplemented with additional GalNAz, and then labeled with tetramethylrhodamine-DIBO (TAMRA-DIBO). The bacteria incorporated newly synthesized carbohydrates into their polysaccharide-rich glycocalyx layer and in most cases displayed both old (AF488-labeled) and newly synthesized carbohydrates, suggesting carbohydrate metabolism is not impaired by MOE-BCC (Fig. 1h).

MOE-BCC labeling targets fluorescence to the glycocalyx

By microscopy (Fig. 1i) and high-resolution 3D rendering (Fig. 1j and Supplementary video 1) we demonstrated that fluorescence localized to the outer surface of *B. fragilis*, consistent with targeting the polysaccharide-rich glycocalyx. To examine whether fluorescence preferentially targeted PSA, we studied wild-type[29](WT) and two mutant strains: ΔPSA, in which a 8-kb deletion of the PSA locus removes essential PSA synthesis genes[29]; and ΔmpiM44[30], which constitutively synthesizes only PSA (Supplementary Table 1). Flow cytometry (Fig. 2a) and confocal microscopy (Fig. 2b) showed AF647-DIBO fluorescence incorporation in both WT and ΔmpiM44 but minimal labeling in the ΔPSA strain. Next, we stained AF647-labeled ΔmpiM44 and ΔPSA with antibodies specific for PSA or *B. fragilis.* The AF647 label co-stained with anti-PSA in ΔmpiM44 but not ΔPSA (Fig. 2c). Western blot showed AF647 fluorescence in conjunction with PSA expression in WT and ΔmpiM44 but not in ΔPSA (Fig. 2d). Taken together, these data suggest that GalNAz is incorporated into PSA, the predominant polysaccharide labeled in *B. fragilis*.

Labeled PSA retains immunomodulatory activity

In MOE-BCC, the fluorescent alkyne preferentially targets PSA. This observation suggested that, in addition to direct visualization of the bacterium, MOE-BCC enables tracking of microbial components, even upon dissociation from intact bacteria. Neither GalNAz incorporation into PSA (Fig. 2e) nor fluorescent labeling of *B. fragilis* (Fig. 2f) affected IL-10 production in dendritic cell (DC)-CD4+ T cell coculture assays (versus native PSA and unlabeled *B. fragilis*, respectively) suggesting MOE-BCC does not ablate PSA's immunomodulatory activity.

Visualization of host–microbe interactions in vitro

We imaged uptake of AF647-labeled *B. fragilis* by primary macrophages *in vitro* (Supplementary Fig. 1a). We observed bacterial uptake, and phagocytic processing as shown by co-staining for early endosomal antigen 1 (EEA-1) and lysosomal-associated membrane protein 1 (LAMP-1). Although fluorescence resided mainly in phagosomes containing bacteria (revealed by DAPI), it was unclear whether the PSA component of AF647-labeled bacteria could detach and be captured by other cells, such as DCs. We pulsed DCs with purified PSA from GalNAz-incorporated *B. fragilis* and observed labeled-PSA accumulation on the DC surface (Supplementary Fig. 1b). In addition, we showed by time-lapse imaging the dynamic uptake of labeled bacteria by macrophages *in vitro* (Supplementary Fig. 1c and Supplementary video 2). Taken together, these data highlight the potential of MOE-BCC in studying dynamic interactions of anaerobic commensal bacteria and their surface glycans with host cells.

Dissemination of labeled bacteria in the host after peritonitis

We next characterized the immune response to AF647-labeled *B. fragilis* injected intraperitoneally into mice, a model of abscess formation and *B. fragilis* release from the intestine as documented in humans[31]. Two hours after infection, ~60% of peritoneal cells were $AF647^{+}$ (Fig. 3a), consisting mainly of macrophages ($SSC^{hi}F4/80^{+/-}$), $MHC\text{-}II^{+}$ cells, and neutrophils; with no differences in cellular composition because of labeling, (Fig. 3a–c).

We used AF647 MFI to infer the amount of labeled bacteria (or PSA) in each subset, and noted CD11b^{+}I-Ab^{+} myeloid cells exhibited the highest MFI, followed by with F4/80^{+} macrophages, neutrophils, CD11c^{+}I-Ab^{+}CD11b^{+} DCs, and F4/80^{-} macrophages. I-Ab^{+}CD11b$^{-/lo}$/c^{-} cells displayed moderate AF647 MFI levels and CD3e^{+} lymphocytes very low levels. Surface expression of I-Ab^{+}CD11b$^{-/lo}$/c^{-} was consistent with peritoneal B cells, suggesting their involvement. We determined that this population, included B-1a (CD5^{+}CD11b^{+}CD43^{+}B220^{lo}), B-1b (CD5^{-}CD11b^{+}CD43^{+}B220^{lo}), and B-2 (CD5^{-}CD11b^{-}CD43^{lo}B220^{hi}) cells, with similar AF647 MFI levels in all subsets (Fig. 3d).

We next investigated the dissemination of labeled *B. fragilis* (and PSA) to the spleen and draining mediastinal lymph nodes (medLNs). In the spleen, we observed an acute response to labeled *B. fragilis*, consisting of macrophages (SSC^{hi}F4/80^{+}), MHC-II^{+} cells, neutrophils, and monocytes/myeloid cells (Fig. 4a). Neutrophils displayed nearly 4-fold higher MFI than any other subset. In draining medLNs, AF647^{+} cells were undetectable at 2 h (data not shown) but were detected in up to ~5% of medLN cells at 7 h. The highest AF647 MFI resided in CD169^{+}CD11b^{+}SSC^{hi}CD11c^{lo} medLN macrophages, which constituted nearly half of the AF647^{+} population (Fig. 4b). Of AF647^{+} cells in medLNs, ~20% were CD19^{+} B cells, which had ~5-fold lower AF647 MFI than medLN macrophages but similar levels to CD169^{-}CD11b^{+} myeloid cells (Fig. 4b). By microscopy we revealed AF647 accumulation in the white-pulp marginal-zone region (Fig. 4c) and along the subcapsular and medullary sinuses of medLNs (Fig. 4e–f). In both areas, fluorescence was confined to regions rich in macrophages and B cells (Fig. 4c–g). In addition to punctate fluorescence, we observed diffuse fluorescence possibly indicative of lysed bacteria and focal release of labeled components like PSA (Fig. 4d,g). Although macrophage uptake of bacteria is expected, the detection of fluorescence in B cells was unexpected. Alternatively, B cells could bind labeled PSA rather than bacteria. To test this, we stained medLN sections with anti-PSA and observed PSA staining in regions with abundant AF647^{+} organisms (Fig. 4f). CD169^{+} macrophages displayed both punctate and diffuse fluorescence, the latter colocalizing with PSA staining (Fig. 4g). To address how B cells acquired fluorescence, we used antibodies specific for whole organisms or PSA. Whereas staining with anti-Bfrag suggested the presence of organisms on the surface of both AF647^{+} macrophages and B cells, staining for PSA was markedly greater on AF647^{+} B cells than macrophages (Fig. 4h). These data suggested that AF647 fluorescence on B cells was attributable more to an association with labeled PSA rather than whole bacteria, and suggest B cells as a potential novel cellular target of PSA after opportunistic infection by *B. fragilis*.

Colonization by labeled anaerobic commensal bacteria in the intestine

We gavaged labeled *B. fragilis* to GF mice and analyzed the lumen of various intestinal segments by flow cytometry. We detected AF647-labeled—but not unlabeled—*B. fragilis* in the small intestine with MFI only slightly reduced from input yet well above autofluorescence (Fig. 5a). We determined the kinetics and regional colonization of *B. fragilis* along the intestinal tract 2 h and 12 h after inoculation. Whereas AF647-labeled *B. fragilis* was detected in the small intestine, bacterial numbers in the colon were low (Fig. 5b). By contrast, at 12 h, organisms in the colon outnumbered those in the small intestine. Indeed, at 2 h, bacterial counts were approximately 80-fold higher in the small intestine than

in the colon (Fig. 5b) however, at 12 h, the ratio was reversed, with *B. fragilis* counts on average more than 40-fold higher in the colon than in the small intestine (Fig. 5b). A decline in MFI at 12 h from that at 2 h suggested bacterial dilution of the AF647 signal, perhaps through proliferation; the increase in bacterial numbers in the colon was consistent with expansion (Fig. 5b). In addition to GF mice, we applied MOE–BCC labeling to track labeled *B. fragilis* in specific pathogen free (SPF) mice, as well as monocolonized mice, which harbor a pre-existing microflora and are perhaps a more clinically-relevant model than GF mice (Fig. 5c). In monocolonized mice, we detected labeled *B. fragilis* in the small intestine at 2 h and the colon at 12 h. This was similar to SPF mice, although the amount of labeled *B. fragilis* in the colon at 2 h was higher. Whether this finding is indicative of altered colonization kinetics or efficiencies in the presence of pre-existing microbiota versus a single bacterial species in gnotobiotic mice, requires further investigation. To further confirm this regional distribution, we examined mice monocolonized with *B. fragilis* from birth, using anti-PSA to determine which intestinal segment harbored *B. fragilis*. Consistent with our previous results, the colon of monocolonized mice contained more *B. fragilis* than the small intestine, implying that *B. fragilis* may preferentially establish a niche in the colon (Fig. 5d).

For visual confirmation, we used intravital two-photon microscopy in live mice[32,33]. We systematically imaged the proximal, medial, and distal segments of the small intestine, and visualized individual fluorescently-labeled *B. fragilis* in the intestinal ileum (Fig. 5c and Supplementary video 3)[32]. In addition, we determined whether MOE-BCC labeling of anaerobic bacteria was compatible with non-invasive whole-body optical imaging We gavaged mice with *B. fragilis* labeled with the near-infrared fluorescent dye cyanine-7 (Cy7). By IVIS (*in vivo* Imaging System), we detected robust fluorescence 6 h after administration in the intestinal region in live and intact GF and SPF mice (Fig. 5f and Supplementary video 4). To examinine the temporal-spatial distribution of labeled *B. fragilis*, we performed longitudinal imaging in intact mice. Fluorescence was maximal between 2 h and 9 h and progressively decreased over time, but was still detectable at 72–96 h compared to baseline (Fig. 5g). To define the spatial distribution of Cy7-labeled *B. fragilis*, we imaged intestinal organs excised from additional GF mice before and after administration (Fig. 5h). At 2 h, the fluorescent signal was strongest primarily in the stomach and in mid- and terminal regions of the small intestine, and by 6 h, it gradually decreased in intensity and became more localized to the ileum and cecum. By 12 h, fluorescence decreased (>5-fold) along the entire intestinal tract and remained in the cecum and colon.

Applicability of MOE–BCC to other gut commensals

We extended MOE–BCC labeling to 14 additional anaerobic commensals (Fig. 6a) and one aerobic pathogen (*Staphylococcus aureus*) (Supplementary Fig. 2). Labeling was highly efficient in 9 (*B. ovatus, B. vulgatus, B. thetaiotaomicron, Prevotella intermedia, Prevotella melaninogenica, Neisseria flavescens, Clostridium difficile, Clostridium ramosum, Lactobacillus reuteri*) of the 14 anaerobes (both gram-negative and gram-positive) from three phyla common in the gut—Bacteroidetes, Firmicutes, and Proteobacteria—and five families (Fig. 6a). Some of these bacteria were better labeled with azido-sugars other than

GalNAz (e.g., *Lactobacillus reuteri* with ManNAz and GlcNAz). These findings suggest that other, still unidentified polysaccharide/carbohydrate moieties may be preferentially labeled in these species.

MOE–BCC labeling exposes species competition in the host intestine

To determine colonization patterns and niche competition, we labeled three gut anaerobic symbionts (*B. fragilis*, *B. ovatus*, and *B. vulgatus*) with separate fluorophores and orally administered them to GF mice (Fig. 6b). We subdivided the small intestine and examined the proximal, medial, and distal segments, as well as cecum and colon. By flow cytometry we detected all three species at varying proportions throughout the intestinal tract (Fig. 6c). *B. ovatus* was present throughout, whereas *B. vulgatus* was very limited in its colonizing capacity and was more abundant in the duodenum (segment 1) of the small intestine (Figs. 6c and Supplementary Fig. 3). Small clusters of fluorescently-labeled *B. vulgatus* were visible by confocal microscopy in the lumen of the small intestine; in contrast, fluorescently labeled *B. fragilis* and *B. ovatus* colonies were more abundant (Fig. 6d). Although the root of this preferential localization is unknown, these data demonstrate that MOE–BCC can be a tool for studying niche preferences of gut commensals.

Discussion

Gut commensals contribute to multiple physiological processes in the host, including immune system modulation[3,34]. We applied MOE-BCC to label and track anaerobic commensals and their polysaccharides in the host in real-time, with no impact on viability, growth, or carbohydrate metabolism. This approach was robust in labeling bacteria and delineated live, proliferating fluorescent bacteria. Despite some loss of fluorescence in bacteria over time, their shed glycans remained permanently labeled until catabolized, presumably by host cells or in the extracellular environment, providing a useful tool for direct tracking of bacterial effector molecules and intact anaerobes.

Discriminating microbe from molecule enables dissection of the role of commensal microorganisms and their metabolites. Using MOE-BCC, we visualized real-time interactions of labeled commensal anaerobic bacteria and molecules shed from their surface, with macrophages *in vitro* and bacterial dissemination along the intestine in live mice. We traced the fate of *B. fragilis* and PSA injected into mice. Resident macrophages as well as infiltrating neutrophils and myeloid cells rapidly responded and phagocytosed labeled *B. fragilis*. Labeled PSA disseminated beyond the infection site: labeled *B. fragilis* was captured by macrophages in the splenic marginal zone and in subcapsular and medullary sinuses of medLNs. These two specialized compartments filter blood and afferent lymphatic fluid, respectively, and are pivotal in stopping the spread of infection and initiating adaptive immune responses to invading microbes[35]. The proximity of these macrophage-rich areas to B cells facilitates recognition and transfer of antigenic material[36]. In spleen and medLNs (as in the peritoneum), we found dimly fluorescent B cells that—stained with anti-PSA—showed evidence for uptake of labeled PSA rather than the whole organism. Primed B cells migrate to the T/B-cell zone, where they solicit help from follicular T-helper cells for immunoglobulin class switching and germinal center formation[37]; how PSA affects this

communication and the overall impact on humoral responses remains unknown. Given the ample evidence that bacterial products affect host immune responses, our approach paves the way toward providing visual proof.

Besides *B. fragilis*, we labeled nine additional commensals and the pathogen *S. aureus*, demonstrating the broad applicability of this labeling method. This method labels anaerobic bacteria, which constitute >99% of microbes colonizing the mammalian intestine and are incompatible with traditional labeling methods. In addition, MOE-BCC provides an alternative for organisms not amenable to genetic manipulation, or to unculturable organisms residing in the intestine.

The *in vivo* labeling and tracking technique described herein allows the determination of bacterial distribution and colonization preferences. We labeled three *Bacteroides* species with different fluorescent colors, and detected and differentiated all three species throughout the intestine. It is yet unkown, whether entire bacteria or only processed molecules traffic to lymphoid tissues and what dynamics underlie trafficking of bacteria or bacterial products to immune compartments. MOE–BCC has a vital part to play in addressing issues such as the role of commensals in mucosal immunology. The ability to track commensals and their immunomodulatory molecules will facilitate elucidation of the critical roles of these entities in immunologic development and disease. Metabolic labeling allows direct tracking of bacterial colonization and dissemination in animals, and also expedites identification of specific cells that participate in regulation of inflammatory or immune responses that might be overlooked with other methods, and may yield strategies to prevent diseases such as autoimmune diseases or inflammatory bowel disorders.

Online Methods

Mice

Male and female 6- to 8-week-old C57BL/6 mice were purchased from Jackson Laboratory or Charles River Laboratories. Swiss Webster mice were purchased from Taconic USA. Mice were housed in specific pathogen–free (SPF) conditions with food and water ad libitum. GF and monocolonized C57BL/6 or Swiss Webster mice were bred and maintained in sterile vinyl isolators in the animal facility at Harvard Medical School and were provided with sterile food (LabDiets® 5K67 and 5021 for C57BL/6 and Swiss Webster mice, respectively), water, and bedding. All experiments were conducted in accordance with National Institutes of Health guidelines and approved by the Harvard Medical Area Standing Committee on Animals.

Bacteria and media

The following bacterial species were used: *Bacteroides fragilis* (NCTC9343), *Bacteroides ovatus* (ATCC8483), *Bacteroides thetaiotaomicron* (ATCC29741), *Bacteroides vulgatus* (ATCC8482), *Prevotella intermedia* (AO10), *Prevotella melaninogenica* (ATCC25845), *Fusobacterium mortiferum* (AO16), *Neisseria flavescens* (SK114), *Clostridium difficile* (AO44), *Clostridium ramosum* (AO31), *Bifidobacterium breve* (SK134), *Bifidobacterium longum* (AO44), *Lactobacillus rhamnosus* (LMS2-1), *Lactobacillus reuteri* (CF48-3A), and *Enterococcus faecalis* (TX0104). *B. fragilis* NCTC9343 was the parent strain for all *B.*

fragilis mutant strains used in these studies (Table 1). All bacteria were grown in a basal peptone-yeast broth containing (per liter) 5 g of yeast extract, 20 g of proteose peptone, 5 g of NaCl, 5 mg of hemin, 0.5 mg of vitamin K1, and 5 g of K_2HPO_4. Hemin, vitamin K1, and K_2HPO_4 were added through a filter after the basal medium had been autoclaved.

Antiserum to *B. fragilis*

Antiserum to *B. fragilis* (anti-Bfrag) was raised in rabbits with the WT strain of *B. fragilis* as previously described[15]. Anti-PSA antiserum was prepared by adsorption of antiserum to WT *B. fragilis* with the ΔPSA *B. fragilis* mutant so that only the anti-PSA fraction within the antiserum remained.

MOE labeling of *B. fragilis*: copper-dependent

B. fragilis was grown overnight at 37°C under anaerobic conditions in 10 ml of the basal medium described above, with or without GalNAz at a final concentration of 100 μM. At an OD_{600} of 0.7, cultures were spun down, washed three times in 1X PBS supplemented with 1% bovine serum albumin (BSA), and labeled with Click-iT® labeling technologies (Invitrogen). The final pellet was resuspended in 500 μl of a reaction mixture (435 μl of 1X Click-iT cell reaction buffer, 10 μl of 100 mM $CuSO_4$, 50 μl of Click-iT cell buffer additive, and 5 μl of either 2 mM AF488 or 2 mM AF647). Bacteria were incubated (while rocking and protected from light) in the reaction mixture for 5 or 30 min, washed four times, and then either used in an experiment or fixed and mounted on a microscope slide with 90% glycerol mounting medium for viewing.

MOE labeling of bacteria: copper-independent

Bacteria were grown overnight at 37°C under anaerobic conditions (80% N_2, 10% H_2, 10% CO_2) in an anaerobic chamber in basal peptone-yeast broth (10, 50, or 100 ml) with GalNAz, GlcNAz, ManNAz, or FucNAz at a final concentration of 100 μM or with either D-galactose or D-GalNAc as a control. When grown in “rich medium,” the broth was supplemented with glucose (0.5%) in addition to the azido sugar. Bacteria were spun down and washed three times in 1X PBS supplemented with 1% BSA. The final pellet was resuspended in 500 μl of 1% BSA in 1X PBS plus 5 μl of 2 mM Click-iT AF488-DIBO, AF647-DIBO, TAMRA-DIBO, or AF488-DIBAC (dibenzoazacyclooctyne) per 10 ml of original culture (final concentration, 20 mM). Each 500-μl volume of this mixture was kept in a separate tube. Tubes were incubated (while rocking and protected from light) for 5 min, 30 min, 2h, 5h, or overnight, after which bacteria were pelleted and washed five times with 3% BSA in 1X PBS. After a final wash, cells were resuspended in 1X PBS and were either used in an experiment or fixed and mounted on a microscope slide with 90% glycerol mounting medium for viewing. For sequential labeling, *B. fragilis* was fluorescently labeled with AF488-DIBO, washed, and grown overnight in basal medium supplemented with additional azido sugars (GalNAz). At an OD_{600} of 0.7, cultures were spun down, re-labeled with TAMRA-DIBO, fixed, and viewed by confocal microscopy.

Tissue culture studies

B. fragilis was grown overnight in medium containing 100 mM GalNAz to an OD_{600} of 0.7 and then labeled by copper-free click-chemistry technology with AF647-DIBO, AF488-DIBO, or TAMRA-DIBO. C57BL/6 primary bone marrow–derived macrophages (5×10^5) were seeded onto 18-mm coverslips in 12-well plates and grown to confluency under humid conditions in an atmosphere of 5% CO_2 at 37°C in RPMI medium supplemented with 10% fetal bovine serum, 1% sodium pyruvate, 1% nonessential amino acids, 1% penicillin/streptomycin, 0.15% sodium bicarbonate, and 2 mM L-glutamine. Cells were washed with 1X PBS, and each well was filled with RPMI medium containing no penicillin/streptomycin. A 10-μl volume of labeled bacterial cells was added to each well. Five hours later, the coverslips were washed twice with RPMI while in the plates. Coverslips were removed from the plates at 5, 15, and 30 min, 1h, and 24 h and were washed three times in 1X PBS. Cells on coverslips were fixed for 10 min in 2% paraformaldehyde and then washed three times in 1X PBS. Cells were permeabilized by incubation with 0.1% Triton X-100 for 5 min, washed twice with 1X PBS, and incubated with LAMP-1 (sc-19992, clone 1D4B, lot H1612) or EEA-1 (sc-6415, clone N-19, lot B1813) antibodies (1:200 in 1% BSA) for 20 min (light-protected) at 37°C. Coverslips were washed twice, mounted on glass slides, and viewed.

DCs were isolated from spleens of untreated mice with CD11c microbeads (Miltenyi), and $CD4^+$ T cells were isolated with a Mouse T Cell CD4 Subset Column Kit (R&D Systems). DCs (2×10^4) were mixed with 10^5 CD4+ T cells in 200 μl of complete RPMI in 96-well round-bottom plates. Cells were cultured with labeled or unlabeled *B. fragilis* and anti-CD3 (1 μg/ml) for 5 days at 37°C in 5% CO_2. IL-10 levels in DC–CD4+ T cell coculture supernatants were measured with a mouse IL-10 DuoSet ELISA Kit (R&D Systems) according to the manufacturer's instructions.

Western blot

B. fragilis cells were labeled with AF647-DIBO as described above. Equal amounts of samples (100 μl from cultures at an OD_{600} of 0.6 ± 0.01) were mixed 1:1 with SDS loading dye, boiled for 5 min, and run on 4–15% stain-free gels. The loading control was measured by imaging of the stain-free gel. SDS gels were then transferred to PVDF membranes. AF647 was detected by the 647-nm fluorescence emitted by the membrane; PSA was detected with *B. fragilis* antiserum specific for this polysaccharide.

Oral administration of labeled bacteria

B. fragilis, *B. ovatus*, and *B. vulgatus* bacteria were grown separately overnight in medium containing GalNAz and then labeled with AF488-DIBO, TAMRA-DIBO, and AF647-DIBO, respectively. After washing as described above and resuspension in 1X PBS, bacteria ($\sim 10^9$) were administered by oral gavage to GF mice (Swiss Webster or C57BL/6). Bacteria in intestinal compartments were analyzed by flow cytometry and/or intravital microscopy 2–7 h after administration. To study the intestinal lumen by flow cytometry, we first removed large cellular debris, protein and lipid material, fecal matter, and food fibers, from intestinal contents by allowing the debris to sediment for ~10 minutes at RT. The upper fluid layer was removed and filtered (40 μm), and washed once in PBS (4750 rpm, 5 min) and resuspended in PBS. Using this method eliminated substantial debris and noise during flow

cytometry analysis of intestinal lumen that would otherwise have masked the transferred bacteria. Samples were run with a low flow rate, on the lowest FSC threshold setting (200). Labeled bacteria were identified using logFSC/logSSC flow cytometry plots and subsequently gated on fluorescence.

B. fragilis peritonitis model

B. fragilis organisms were grown in medium containing GalNAz and labeled with AF647-DIBO by the copper-free method as described above. Approximately 10^7–10^8 organisms were injected IP into SPF C57BL/6 mice. At 2 h and 7 h after injection, mice were euthanized with CO_2, the peritoneum was lavaged with 5 ml of PBS, and the spleen and draining medLNs were removed. Lavage, spleen, and medLN cell suspensions were filtered through nylon mesh, resuspended in cell-staining buffer (BioLegend), and subsequently stained with anti-CD16/CD32 (clone 2.4G2, BioXcell) for 5 min on ice to block nonspecific staining via Fc receptor uptake of antibodies. This process was followed by staining on ice for 20 min (at 1:200 dilution) with fluorescently labeled antibodies (BioLegend or eBioscience) to CD3e (145-2C11), CD5 (53–7.3), CD11b (M1/70), CD11c (N418 or HL3), CD19 (6D5), CD43 (eBioR2/60), B220 (RA3-6B2), F4/80 (BM8), I-Ab (AF6-120.1), Ly6C (HK1.4), Ly6G (1A8), or TER-119 (TER-119). The stained samples were acquired by flow cytometry (Canto, Canto-II, or LSR-II; all from BD Biosciences) and analyzed with FlowJo software. For cryosectioning, harvested spleens and medLNs were fixed overnight at 4°C in phosphate-buffered L-lysine with 1% paraformaldehyde/periodate (PLP) solution and cryoprotected by transfer to 10%, 20%, and 30% sucrose solutions (in PBS) daily. Tissues were then rinsed several times in PBS, embedded in TBS^{TM} Tissue-Freezing Medium (Triangle Biomedical Sciences), frozen into tissue molds, and later sectioned at a thickness of ~20–30 μm with a cryostat. The spleen and medLN sections were next incubated with purified (or, where applicable, fluorescently conjugated) primary antibodies at room temperature or 4°C for 1–2 h, after which they were extensively washed with PBS and incubated again with fluorescently conjugated secondary antibodies (where applicable). Slides were extensively washed and stained for 10 min with DAPI nuclear stain (1 μg/ml). Confocal images were acquired with an Olympus Fluoview BX50WI inverted confocal microscope using a 10×/0.4 numerical aperture (NA) and a 20×/0.5-NA or 60×/1.42-NA objective. Images were processed with Volocity software (PerkinElmer).

Intravital two-photon microscopy of the intestine

For intestine imaging, mice (8–10 weeks old; GF, Swiss Webster) were given 10^9 fluorescence-labeled bacteria by oral gavage at least 6 h prior to imaging. Intravital two-photon microscopy of the murine intestine was performed as previously described[32]. Given the thickness of the cecum and colonic muscularis, which impedes fluorescence, we focused on imaging the small intestine at acute time points of optimal bacterial fluorescence. Mice were anesthetized with ketamine, xylazine, and acepromazine and positioned on a customized heated stage. A ~1cm segment of intestine was exteriorized through the peritoneum, immobilized with tissue-adhesive glue, and kept hydrated by a mixture of PBS/lubricant gel. In some preparations, labeled bacteria were injected directly into the intestinal loop. For *in vivo* nuclear staining, mice received Hoechst 33342 (Sigma; 10 mg/kg i.v.) at least 1h before imaging to counterstain the nuclei of the intestinal epithelium thereby

delineating the villi. Two-photon imaging was performed on an Ultima Two-Photon Microscope (Prairie Technologies) equipped with a Tsunami Ti:sapphire laser with a 10-W MilleniaXs pump laser (Spectra-Physics) and a 20× (0.95NA) water immersion objective (Olympus). Background autofluorescence was minimized by having mice on a non-fluorescent diet (alfalfa-free) at least one week prior to imaging. In addition, background fluorescence was minimized by tuning the two-photon excitation wavelength to 900–940 nm for optimal fluorescence excitation of bacteria while limiting excitation of autofluorescent material in the intestine. Fluorescence was detected with 450/50-nm, 525/50-nm, 590/50-nm, and 665/65-nm bandpass filters for four-color imaging. Image sequences were transformed into volume-rendered Z-stacks with Volocity software (Improvision).

Time-lapse phagocytosis imaging

Murine bone marrow–derived macrophages were cultured overnight in optical imaging chambers (Ibidi) in 10% FBS in phenol red-free RPMI (Cellgro). After overnight adherence, fresh medium was provided; AF488-labeled *B. fragilis* was subsequently added to the macrophage imaging culture chamber and transferred to a VivaView Live Cell Imaging incubator outfitted with a fully integrated and motorized inverted microscope running on Metamorph software. Images were captured with a 40x objective in GFP and DIC channels at 1-min intervals for approximately 12h. Videos were compiled with Volocity software.

Whole-body *in vivo* optical imaging

In Vivo Imaging System (IVIS) Spectrum (PerkinElmer) was used for serial *in vivo* live whole-body imaging. The IVIS machine is equipped with 10 narrow-band excitation filters (30-nm bandwidth) and 18 narrow-band emission filters (20-nm bandwidth). Mice were gavaged with Cy7 labeled *B. fragilis* at t = 0 and anesthetized with isoflurane administered by vaporizer at every time point. Mice were subjected to imaging with IVIS Spectrum by setting Ex=745 nm; Em=800-nm filters; and FOV=C. Imaging reconstruction and analysis were performed with Living Image version 4.3.1/4.4.

Statistical analyses

All statistical analyses in this study were performed with Prism (GraphPad Software) and based on normally distributed data sets with equal variance (Bartlett's test). Gender- and age-matched mice were randomly assigned to groups for *in vivo* experiments, and no data points were excluded. Investigators were not blinded during the experiments or outcome assessment. Where applicable, data points were presented as mean ± s.d. values unless otherwise stated. Data were inferred as statistically significant if P values were <0.05. Significance between two groups was determined by two-tailed unpaired Student's t-test. For multiple comparisons, one-way ANOVA was used with Tukey's multiple comparisons post hoc test unless stated otherwise.

Supplementary Material

Refer to Web version on PubMed Central for supplementary material.

Acknowledgments

We thank the Neurobiology Imaging Facility for consultation and instrument availability that supported this work. This facility is supported in part by the Neural Imaging Center as part of an NINDS P30 Core Center grant #NS072030. We also like to thank: Dr. Natasha Barteneva of the Flow and Imaging Cytometry Resource for help in whole-body imaging on the IVIS Spectrum (funded by NIH 1 S10 OD016401 and BCH/PCMM); Julie Czupryna and Marc Guerra from PerkinElmer for consultation and expert advice; Chad Araneo (Division of Immunology Flow Cytometry Core Facility, HMS) and Dr. Laurie Comstock for helpful discussions, comments and reagents; as well as members of the Kasper and von Andrian lab for helpful discussions. This work was also partly supported by National Institutes of Health grants to U.H.vA (PO1 AI111595) and D.A (5T32 HL066987). Additional support to U.H.vA. was provided by U19AI095261 and the Ragon Institute at MGH, MIT, and Harvard. N.G-Z. was supported by an EMBO Long-Term Fellowship (ALTF 251-2011), the Human Frontiers Science Program (LT000079/2012), a UNESCO L'Oreal National and International Women in Science Award, a Fulbright, and the Weizmann Institute of Science–National Postdoctoral Award Program for Advancing Women in Science. J.E.H. was supported by the Cancer Research Institute Irvington Fellowship Program and N.C.R. by the departmental Kirschstein-NRSA training grant.

References

1. Structure, function and diversity of the healthy human microbiome. Nature. 2012; 486:207–214.10.1038/nature11234 [PubMed: 22699609]
2. Turnbaugh PJ, et al. The human microbiome project. Nature. 2007; 449:804–810.10.1038/nature06244 [PubMed: 17943116]
3. Hooper LV, Littman DR, Macpherson AJ. Interactions between the microbiota and the immune system. Science. 2012; 336:1268–1273.10.1126/science.1223490 [PubMed: 22674334]
4. Ivanov II, Littman DR. Modulation of immune homeostasis by commensal bacteria. Current opinion in microbiology. 2011; 14:106–114.10.1016/j.mib.2010.12.003 [PubMed: 21215684]
5. Atarashi K, et al. Treg induction by a rationally selected mixture of Clostridia strains from the human microbiota. Nature. 2013; 500:232–236.10.1038/nature12331 [PubMed: 23842501]
6. Ahern PP, Faith JJ, Gordon JI. Mining the human gut microbiota for effector strains that shape the immune system. Immunity. 2014; 40:815–823.10.1016/j.immuni.2014.05.012 [PubMed: 24950201]
7. Atarashi K, et al. Induction of colonic regulatory T cells by indigenous Clostridium species. Science. 2011; 331:337–341.10.1126/science.1198469 [PubMed: 21205640]
8. Ivanov, et al. Induction of intestinal Th17 cells by segmented filamentous bacteria. Cell. 2009; 139:485–498.10.1016/j.cell.2009.09.033 [PubMed: 19836068]
9. An D, et al. Sphingolipids from a symbiotic microbe regulate homeostasis of host intestinal natural killer T cells. Cell. 2014; 156:123–133.10.1016/j.cell.2013.11.042 [PubMed: 24439373]
10. Dasgupta S, Kasper DL. Relevance of commensal microbiota in the treatment and prevention of inflammatory bowel disease. Inflammatory bowel diseases. 2013; 19:2478–2489.10.1097/MIB.0b013e318297d884 [PubMed: 23846489]
11. Yurkovetskiy LA, Pickard JM, Chervonsky AV. Microbiota and Autoimmunity: Exploring New Avenues. Cell host & microbe. 2015; 17:548–552.10.1016/j.chom.2015.04.010 [PubMed: 25974297]
12. Sommer F, Backhed F. The gut microbiota--masters of host development and physiology. Nature reviews. Microbiology. 2013; 11:227–238.10.1038/nrmicro2974 [PubMed: 23435359]
13. Surana NK, Kasper DL. The yin yang of bacterial polysaccharides: lessons learned from B. fragilis PSA. Immunological reviews. 2012; 245:13–26.10.1111/j.1600-065X.2011.01075.x [PubMed: 22168411]
14. Mazmanian SK, Liu CH, Tzianabos AO, Kasper DL. An immunomodulatory molecule of symbiotic bacteria directs maturation of the host immune system. Cell. 2005; 122:107–118.10.1016/j.cell.2005.05.007 [PubMed: 16009137]
15. Krinos CM, et al. Extensive surface diversity of a commensal microorganism by multiple DNA inversions. Nature. 2001; 414:555–558.10.1038/35107092 [PubMed: 11734857]
16. Coyne MJ, Chatzidaki-Livanis M, Paoletti LC, Comstock LE. Role of glycan synthesis in colonization of the mammalian gut by the bacterial symbiont Bacteroides fragilis. Proceedings of

the National Academy of Sciences of the United States of America. 2008; 105:13099–13104.10.1073/pnas.0804220105 [PubMed: 18723678]

17. Dasgupta S, Erturk-Hasdemir D, Ochoa-Reparaz J, Reinecker HC, Kasper DL. Plasmacytoid dendritic cells mediate anti-inflammatory responses to a gut commensal molecule via both innate and adaptive mechanisms. Cell host & microbe. 2014; 15:413–423.10.1016/j.chom.2014.03.006 [PubMed: 24721570]
18. Ochoa-Reparaz J, et al. A polysaccharide from the human commensal Bacteroides fragilis protects against CNS demyelinating disease. Mucosal immunology. 2010; 3:487–495.10.1038/mi.2010.29 [PubMed: 20531465]
19. Tsien RY. The green fluorescent protein. Annual review of biochemistry. 1998; 67:509–544.10.1146/annurev.biochem.67.1.509
20. Craggs TD. Green fluorescent protein: structure, folding and chromophore maturation. Chemical Society reviews. 2009; 38:2865–2875.10.1039/b903641p [PubMed: 19771333]
21. Boyce M, Bertozzi CR. Bringing chemistry to life. Nature methods. 2011; 8:638–642.10.1038/nmeth.1657 [PubMed: 21799498]
22. Sletten EM, Bertozzi CR. Bioorthogonal chemistry: fishing for selectivity in a sea of functionality. Angew Chem Int Ed Engl. 2009; 48:6974–6998.10.1002/anie.200900942 [PubMed: 19714693]
23. Dehnert KW, et al. Metabolic labeling of fucosylated glycans in developing zebrafish. ACS chemical biology. 2011; 6:547–552.10.1021/cb100284d [PubMed: 21425872]
24. Dumont A, Malleron A, Awwad M, Dukan S, Vauzeilles B. Click-mediated labeling of bacterial membranes through metabolic modification of the lipopolysaccharide inner core. Angew Chem Int Ed Engl. 2012; 51:3143–3146.10.1002/anie.201108127 [PubMed: 22323101]
25. Kaewsapsak P, Esonu O, Dube DH. Recruiting the host's immune system to target Helicobacter pylori's surface glycans. Chembiochem : a European journal of chemical biology. 2013; 14:721–726.10.1002/cbic.201300006 [PubMed: 23512824]
26. Cobb BA, Kasper DL. Characteristics of carbohydrate antigen binding to the presentation protein HLA-DR. Glycobiology. 2008; 18:707–718.10.1093/glycob/cwn050 [PubMed: 18525076]
27. Hawkins ED, et al. Measuring lymphocyte proliferation, survival and differentiation using CFSE time-series data. Nature protocols. 2007; 2:2057–2067.10.1038/nprot.2007.297 [PubMed: 17853861]
28. Troy EB, Carey VJ, Kasper DL, Comstock LE. Orientations of the Bacteroides fragilis capsular polysaccharide biosynthesis locus promoters during symbiosis and infection. Journal of bacteriology. 2010; 192:5832–5836.10.1128/JB.00555-10 [PubMed: 20729352]
29. Coyne MJ, et al. Polysaccharide biosynthesis locus required for virulence of Bacteroides fragilis. Infection and immunity. 2001; 69:4342–4350.10.1128/IAI.69.7.4342-4350.2001 [PubMed: 11401972]
30. Coyne MJ, Weinacht KG, Krinos CM, Comstock LE. Mpi recombinase globally modulates the surface architecture of a human commensal bacterium. Proceedings of the National Academy of Sciences of the United States of America. 2003; 100:10446–10451.10.1073/pnas.1832655100 [PubMed: 12915735]
31. Nord CE. Incidence and significance of intraperitoneal aerobic and anaerobic bacteria. Clinical therapeutics. 1990; 12(Suppl B):9–20. [PubMed: 2196123]
32. Millet YA, et al. Insights into Vibrio cholerae intestinal colonization from monitoring fluorescently labeled bacteria. PLoS pathogens. 2014; 10:e1004405.10.1371/journal.ppat.1004405 [PubMed: 25275396]
33. Farache J, Zigmond E, Shakhar G, Jung S. Contributions of dendritic cells and macrophages to intestinal homeostasis and immune defense. Immunology and cell biology. 2013; 91:232–239.10.1038/icb.2012.79 [PubMed: 23399695]
34. Dethlefsen L, McFall-Ngai M, Relman DA. An ecological and evolutionary perspective on human-microbe mutualism and disease. Nature. 2007; 449:811–818.10.1038/nature06245 [PubMed: 17943117]
35. Martinez-Pomares L, Gordon S. CD169+ macrophages at the crossroads of antigen presentation. Trends in immunology. 2012; 33:66–70.10.1016/j.it.2011.11.001 [PubMed: 22192781]

36. Cyster JG. B cell follicles and antigen encounters of the third kind. Nature immunology. 2010; 11:989–996.10.1038/ni.1946 [PubMed: 20959804]

37. Vinuesa CG, Linterman MA, Goodnow CC, Randall KL. T cells and follicular dendritic cells in germinal center B-cell formation and selection. Immunological reviews. 2010; 237:72–89.10.1111/j.1600-065X.2010.00937.x [PubMed: 20727030]

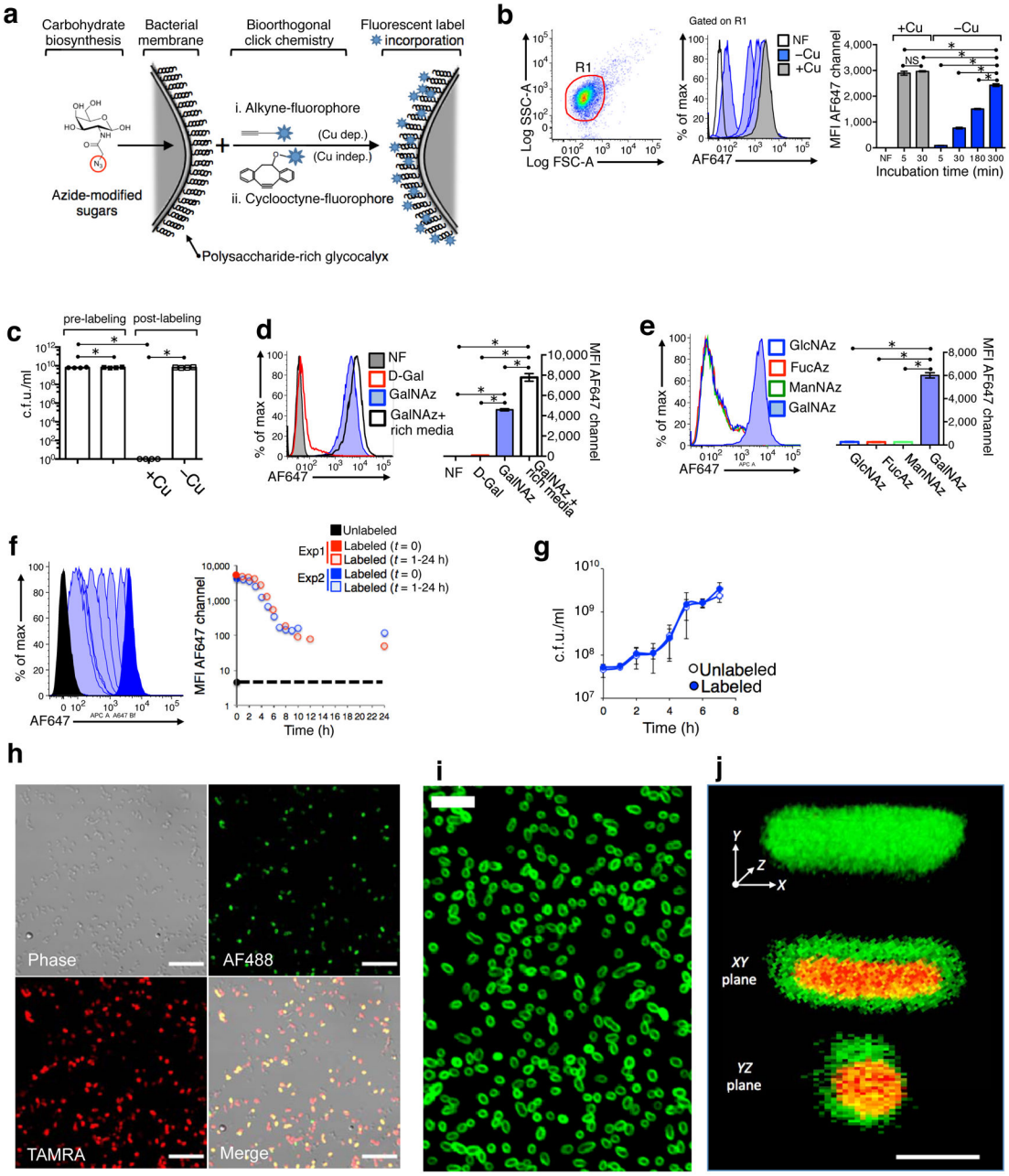

Figure 1. Generation of fluorescent anaerobic commensal gut bacteria by MOE and BCC

(**a**) Schematic of MOE–BCC approach incorporating azide-modified sugars into carbohydrates with subsequent fluorescent labeling via copper-dependent (Cu dep.) and -independent (Cu indep.) reactions. (**b**) Flow cytometry plots of labeled *B. fragilis* (left) and AF647 MFI quantification (right) upon increased labeling time with or without copper. (**c**) Viability counts of *B. fragilis* before and after labeling with or without copper. Data are mean±sem; *P<0.05; one-way ANOVA; n = 4. (**d**) Flow-cytometry of labeled *B. fragilis* (left) and MFI (right) grown in media supplemented with D-galactose or azide-modified analogs (GalNAz) in the presence (+ rich media) or absence of competing substrates. (**e**)

Flow-cytometry of labeled *B. fragilis* (left) and MFI (right) after growth with various azide-modified sugars.(**f**) Change in fluorescence intensity over time after initial BCC labeling at $t = 0$ with intermittent sampling to determine MFI for up to 24 h.(**g**) Growth curves comparing unlabeled with fluorescence-labeled *B. fragilis* under optimal growth conditions. (**h**) Polysaccharide turnover after sequential labeling of *B. fragilis*. Representative images depict TAMRA (red, top left), AF488 (green, top right), merged (yellow, bottom right), and individual bacteria in phase (bottom left). Scale bar, 10 μm. (**i**) Confocal microscopy of AF488-labeled *B. fragilis* grown with D-GalNAz. Scale bar, 5 μm.(**j**) 3D rendered confocal image of AF488-labeled *B. fragilis* counterstained with propidium-iodide for DNA. Scale bar, 1 μm. Data in b,c,d,e are representative of at least three independent experiments.

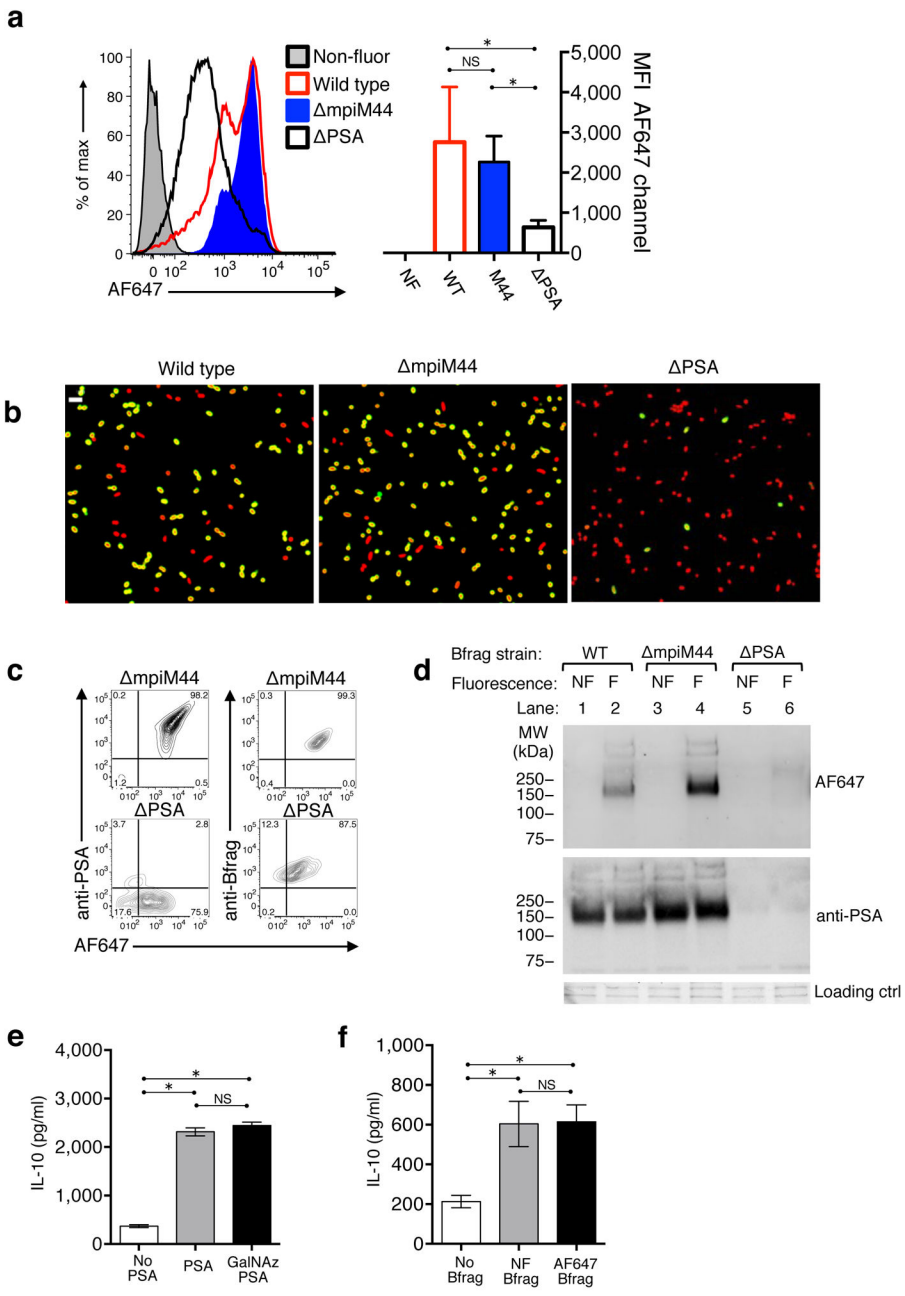

Figure 2. MOE–BCC labeling preserves the immunoregulatory activity of PSA in *B. fragilis*

(**a**) Flow cytometry plots (left) and MFI quantification (right) of WT *B. fragilis* and mutant strains ΔmpiM44 (PSA-exclusive) and ΔPSA (PSA-deficient) after fluorescent labeling under growth conditions supplemented with GalNAz. (**b**) Confocal images of fluorescence-labeled WT *B. fragilis* and mutant strains ΔmpiM44 and ΔPSA after MOE labeling with AF488-DIBO (green) and counterstaining with propidium-iodide (red). Scale bar, 3 μm. (**c**) Flow cytometry analysis of anti-PSA and anti-*B. fragilis* reactivity to AF647-labeled *B. fragilis*. Mutant strains ΔmpiM44 and ΔPSA were fluorescently labeled as in (**a**) with AF647-DIBO and then stained with antisera to PSA (anti-PSA) or *B. fragilis* (anti-Bfrag)

followed by fluorescently labeled secondary antibody. (**d**) Western blot analysis of AF647-labeled *B. fragilis* strains (WT, ΔmpiM44, and ΔPSA). Inactivated, labeled bacteria were run on stain-free SDS gels (for the loading control), visualized on the AF647 channel to identify AF647-labeled bands, and blotted with anti-PSA. NF, non-fluorescent; F, fluorescent. (**e**) IL-10 levels from DC–$CD4^+$ T cell cocultures after polyclonal stimulation with anti-CD3 in the presence of native PSA, GalNAz-incorporated PSA (GalNAz PSA), or no PSA. Data are mean ± s.e.m. values (n=3). * $P<0.05$ using one-way ANOVA. (**f**) IL-10 levels from DC–$CD4^+$ T cell cocultures after polyclonal stimulation with anti-CD3 in the presence of unlabeled *B. fragilis*, AF647-labeled *B. fragilis*, or no bacteria. Data are mean ± s.e.m. values (n=4). * $P<0.05$ using one-way ANOVA. Data in (**a–f**) are representatives of 3 experiments, and (**c**) representative of 2 experiments.

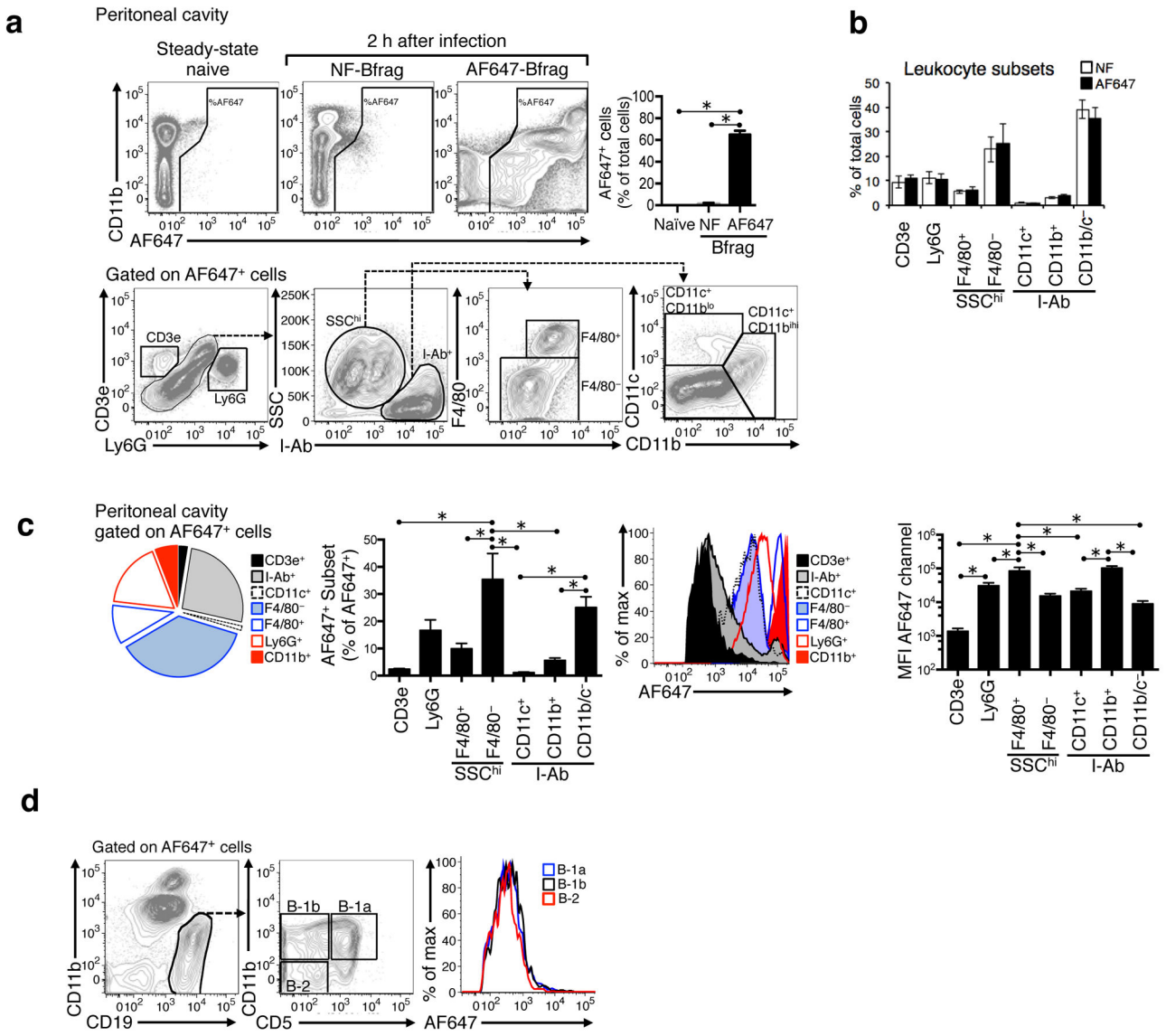

Figure 3. In vivo uptake of AF647-labeled *B. fragilis* after acute infection

(**a**) Flow cytometry gating strategy and frequency (top right) of AF647$^+$ cells in the peritoneum 2 h after acute infection with non-fluorescent (NF) or fluorescence-labeled *B. fragilis* (AF647-Bfrag) and naïve controls. Bottom row shows gating strategy among AF647$^+$ cells, depicting lymphocytes (CD3e), neutrophils (Ly6G), F4/80$^{+/-}$ macrophages, CD11c$^+$ DCs, CD11b$^+$ myeloid/monocytic cells, and I-Ab$^+$ cells. * P<0.05 using one-way ANOVA.(**b**) Comparison of leukocyte subset frequencies in the peritoneum 2 h after acute infection with NF or AF647-Bfrag. Results for NF and AF647 are not statistically significant by t-test..(**c**) Pie-chart analysis and bar graph show frequency (left) and MFI (right) of AF647$^+$ leukocyte subsets in the peritoneum 2 h after acute infection. Data in (**a–c**) represent three independent experiments (n=3–4 per experiment). * P<0.05 using one-way ANOVA (**d**) Peritoneal B-cell subset analysis of AF647$^+$ cells recovered from the peritoneum 2 h after acute infection with AF647-labeled *B. fragilis*. Gated CD19$^+$AF647$^+$

cells were examined for prototypical B-1a ($CD11b^{+}CD5^{+}$), B-1b ($CD11b^{+}CD5^{-}$), and B-2 ($CD11b^{-}CD5^{-}$) markers and were analyzed for MFI of the AF647 channel. Data representative of at least three independent experiments.

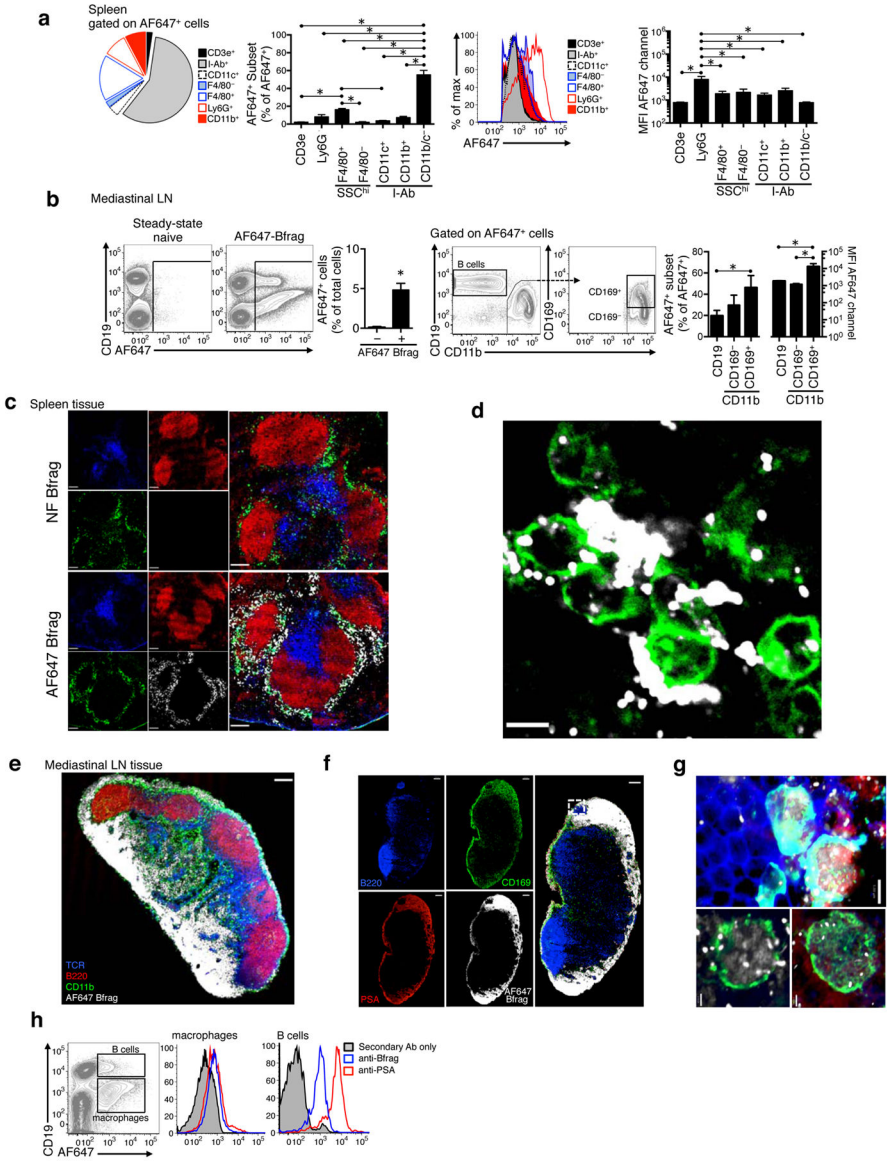

Figure 4. Dissemination of AF647-labeled *B. fragilis* and PSA to secondary lymphoid organs

(**a**) Pie-chart analysis and bar graph showing frequency (left) and MFI (right) of AF647$^+$ leukocytes in the spleen 2 h after acute infection with fluorescence-labeled *B. fragilis*. (**b**) Flow cytometry analysis and frequency (left) of total AF647$^+$ cells recovered from mediastinal LNs 7 h after AF647 Bfrag infection versus control mice. Gating strategy for AF647$^+$ B cells and macrophages (middle) and AF647$^+$ MFI analysis on AF647$^+$ cells (right)..(**c**) Confocal images of spleen tissue 2 h after infection with non-fluorescent (NF; top) or AF647$^+$ Bfrag (bottom). Individual (left) and merged (right) images depict T-cells (TCRβ, blue), B-cells (B220, red), macrophage/myeloid cells (CD11b, green), and AF647$^+$-labeled *B. fragilis* (white). Scale bar, 100 μm. (**d**) Zoomed image of AF647$^+$ Bfrag (white) and macrophages (green) in the splenic white pulp. Scale bar, 5 μm. (**e**) Confocal image of mediastinal LN 7 h after challenge with AF647$^+$ Bfrag, depicting T-cells (blue), B-cells (red), macrophages (green) and AF647$^+$-labeled *B. fragilis* (white). Scale bar, 100 μm. (**f**)

Individual (left) and merged (right) images depict B-cells (blue), CD169+ macrophages (green), anti-PSA staining (red), and AF647^{+}-labeled *B. fragilis* (white). Scale bar, 100 μm. (**g**) Zoomed confocal image (top) from boxed area in (**f**) depicting AF647^{+} Bfrag (white), CD169^{+} macrophages (green), B cells (blue), and diffuse PSA staining (red). Scale bar, 5 μm. Bottom panels depict zoomed images of CD169^{+} macrophages (green) and AF647 Bfrag (white) with (bottom right) or without (bottom left) anti-PSA staining (red). Scale bar, 2 μm.(**h**) Flow cytometry analysis of anti–*B. fragilis* and anti-PSA staining on gated AF647^{+} B cells and macrophages recovered from LNs 7 h after infection. Data in (**a,b**) show mean ±s.e.m. of (n=4 mice) and representative of three independent experiments. *P<0.05 using one-way ANOVA.

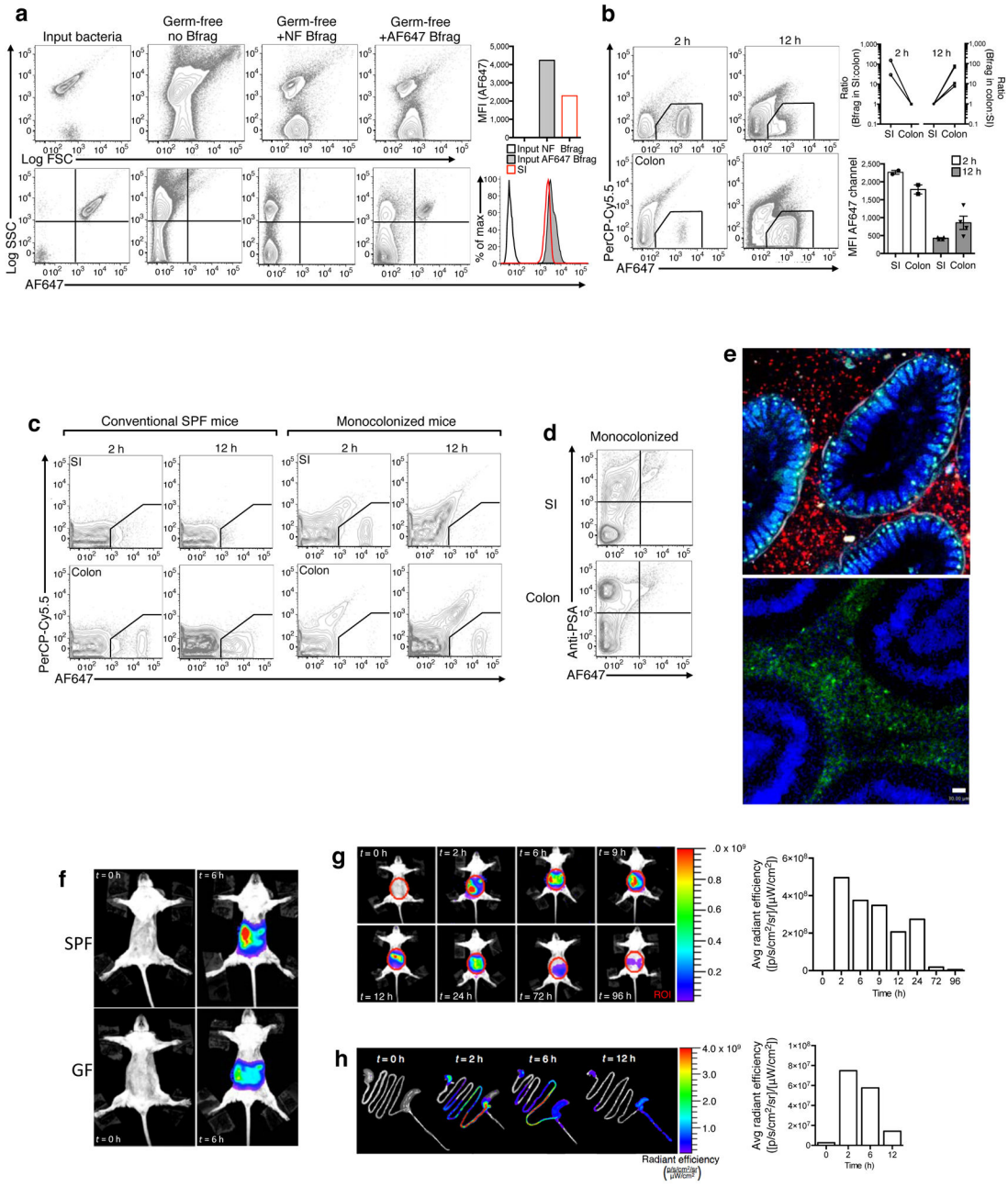

Figure 5. In vivo tracking and visualization of *B. fragilis* in the intestine

(**a**) Flow cytometry of intestinal lumen from GF mice gavaged with nonfluorescent (NF) or AF647-labeled (AF647) *B. fragilis* versus naïve GF mice. Bar graph (top right) and flow cytometry histogram (bottom right) of AF647 MFI levels on recovered Bfrag from small intestine (SI). Data representative of two independent experiments. (**b**) Flow cytometry detection of AF647 Bfrag in the SI and colon (left). Quantification of AF647 Bfrag (top right) from the SI versus colon expressed as the fold change in ratios of bacteria found in SI to colon (at 2 h) or colon to SI (at 12 h). AF647 MFI levels of bacteria recovered from SI and colon (bottom right). Data show individual raw data points (n=2–4 mice). (**c**) Tracking

labeled *B. fragilis* in conventional SPF and monocolonized mice. (n=4) (**d**) Preferential colonization of *B. fragilis* in the colon (bottom) versus SI (top) in mice monocolonized with *B. fragilis*. (**e**) Representative images from intravital two-photon microscopy of the SI after inoculation with TAMRA-labeled (top) or AF488–labeled (bottom) *B. fragilis*. Blue denotes Hoechst nuclear dye. See Supplementary Video 3. (**f–h**) Whole body imaging by IVIS, following administration of Cy7-labeled *B. fragilis* in conventional SPF (**f**) and GF mice (**f–h**). Longitudinal imaging (**g**) and imaging of dissected intestines (**h**) following administration of Cy7-labeled *B. fragilis*. Bar graphs (right) show quantification of fluorescence as average radiant efficiency taken at each of the indicated time points.

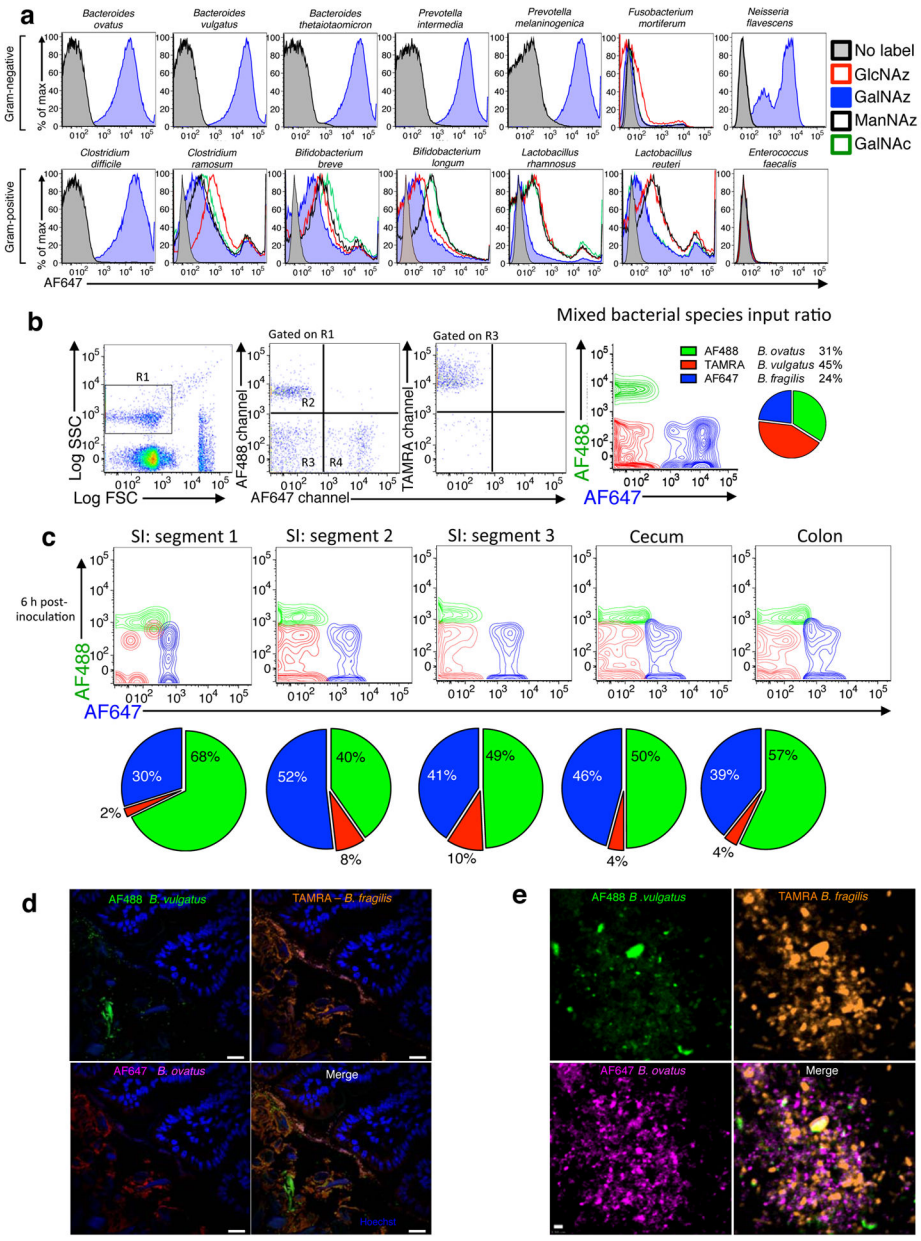

Figure 6. Labeling of various anaerobic gut commensals and assessment of species competition

(**a**) Flow cytometry histograms showing AF647 fluorescence following labeling in 9 of 14 gram-negative (top row) and gram-positive (bottom row) bacteria from 3 phyla and 5 families. For bacteria showing poor labeling efficiency with GalNAz, we tested additional azide-modified sugars: GlcNAz, ManNAz, and GalNAc. (**b**) Oral delivery of three members of *Bacteroidetes. B. fragilis*, *B. ovatus*, and *B. vulgatus* were grown with GalNAz and labeled with AF647-DIBO, AF488-DIBO, and TAMRA-DIBO, respectively. Bacteria were mixed and the frequency of each species was determined by flow cytometry (left) and computed as an input ratio (right). (**c**) Flow cytometry detection (top) of labeled bacteria from lumen suspensions of the proximal (segment 1), medial (segment 2), and distal (segment 3) regions of the small intestine (SI) as well as from the cecum and colon, 6 h after

oral delivery. Individual pie charts (bottom) show relative counts of each species expressed as a percentage of all bacteria recovered. (**d,e**) Confocal images of the ileum colonized with the mixture of labeled bacteria from a technical repeat of (**c**), where the fluorescent dyes were swapped to negate detrimental affects of the fluorescent label. In (**d,e**) *B. vulgatus* was labeled with AF488 (green), *B. fragilis* with TAMRA (orange), and *B. ovatus* with AF647 (magenta); DNA was labeled with Hoechst (blue). Scale bar, 10 μm. (e) Zoomed images depict labeled bacteria in the ileum. Scale bar, 1.8 μm). Data are representative of two independent experiments.